Molecular Vision 2017; 23:431-446 <http://www.molvis.org/molvis/v23/431>
Received 31 January 2017 | Accepted 14 July 2017 | Published 17 July 2017

Physical disruption of cell–cell contact induces VEGF expression in RPE cells

Farhad Farjood, Elizabeth Vargis

Department of Biological Engineering, Utah State University, Logan, UT

Purpose: To investigate the role of RPE cell–cell contact in vascular endothelial growth factor (VEGF) protein expression in cultures of primary human RPE (hRPE) cells and a human RPE cell line (ARPE-19).
Methods: Two in vitro methods, scratching and micropatterning, were used to control the physical dissociation of RPE cell–cell junctions. Scratching was performed by scoring monolayers of RPE cells with a cell scraper. Micropatterning was achieved by using a stencil patterning method. Extracellular VEGF expression was assessed by using an enzyme-linked immunosorbent assay (ELISA) kit. Immunocytochemistry (ICC) was performed to visualize the expression and localization of VEGF and intercellular proteins zonula occludens-1 (ZO-1), N-cadherin, β-catenin, and claudin-1 in RPE cultures.
Results: Higher expression of VEGF protein by cells on the edges of the scratched RPE layers was confirmed with ICC in short-term (1 day after confluency) and long-term (4 weeks after confluency) cultures. According to the ICC results, ZO-1, N-cadherin, β-catenin, and claudin-1 successfully localized to cell–cell junctions in long-term cultures of ARPE-19 and hRPE cells. However, unlike N-cadherin, β-catenin, and claudin-1, only ZO-1 localized junctionally in short-term cultures of both cell types. Moreover, removing cell–cell junctions by scratching resulted in the delocalization of ZO-1 from tight junctions to the cytoplasm. The loss of tight junction formation and the accumulation of ZO-1 in the cytoplasm correlated with increased VEGF expression. Micropatterning RPE cells on different sized circular patterns produced varying concentrations of cells with lost cell–cell junctions. When fewer cells formed intercellular junctions, increased extracellular VEGF secretion was observed from the ARPE-19 and hRPE cells.
Conclusions: VEGF expression increases after physical disruption of RPE cell–cell connections. This increase in VEGF expression correlates with the loss of intercellular junctions and the localization of ZO-1 in the cytoplasm of RPE cells.

The exudative (wet) form of age-related macular degeneration (AMD) is characterized by the abnormal growth of new leaky blood vessels in the choroid (choroidal neovascularization, CNV) and near the macula. CNV can cause RPE deformation and degeneration, leading to the irreversible loss of vision [1,2]. Although the exact causes of CNV are not completely understood, RPE-derived vascular endothelial growth factor (VEGF), a potent angiogenesis factor, is generally thought to be the major stimulator of CNV [3-10].

Appropriate levels of VEGF are crucial for the normal development of the choroid [11,12]. VEGF also functions as an important factor in maintaining RPE and endothelial cells [11]. However, abnormal levels of VEGF are also associated with retinal disease [3]. Moreover, overexpressing VEGF in rat RPE results in the development of CNV [4,5]. Accordingly, VEGF has been the foremost target in many experimental studies and clinical trials to inhibit CNV. The most successful treatment for CNV in wet AMD uses recombinant anti-VEGF to antagonize VEGF, slow vision loss, and improve visual acuity [6-10].

Even though anti-VEGF products slow the progression of CNV, there is no cure or prevention for CNV associated with wet AMD. The exact mechanisms resulting in the overexpression of angiogenic factors, including VEGF, in RPE cells remain unknown. A wide range of molecular and environmental factors has been implicated in elevated VEGF expression by RPE cells, including hypoxia [13-16] and inflammation due to increased levels of inflammatory cytokines or drusen components, such as C3a, C5a, and amyloid β [17-19].

Reduced RPE cell–cell adhesion, caused by RPE tears or RPE cell death in the latest stages of dry AMD, may also elevate VEGF gene expression. RPE tears occur during AMD from RPE detachment or CNV [20-24] and most commonly from intravitreal injection of anti-VEGF drugs during treatment [24-28]. RPE cell death, mediated by apoptosis and/or necrosis, in geographic atrophy (GA) is another in vivo phenomenon through which the physical contact between RPE cells is lost [29-31]. Two separate studies reported increased mRNA levels of VEGF after calcium-mediated dissociation of RPE cell–cell junctions [32,33].

Correspondence to: Elizabeth Vargis, Department of Biological Engineering, Utah State University, 4105 Old Main Hill, Logan, UT 84322; Phone: (435) 797-0618; FAX: (435) 797-1248; email: vargis@usu.edu

However, because the exact effect of extracellular calcium ions on VEGF expression is unclear, alternative in vitro methods may elucidate the role of physical cell–cell adhesion in VEGF expression. Moreover, none of these studies, to our knowledge, has demonstrated how junctional cell–cell detachment affects the expression of the VEGF protein. In this work, we used two in vitro methods, scratching and micropatterning, without introducing exogenous components to study the role of RPE cell–cell adhesion in VEGF protein expression.

Scratching assays, also known as wound healing assays, are generally used to mimic tissue damage and study the proliferation and migration capability of cells [34,35]. Scratching has also been used to study the molecular events associated with the loss of cell–cell contact in RPE cells [36]. Specifically, the expression of platelet-derived growth factor (PDGF) increased in cells on the leading edge of a scratched RPE layer [37]. Another analysis demonstrated that scratching a monolayer of ARPE-19 cells altered the expression of the genes encoding hepatoma-derived growth factor (HDGF), mitogen-activated protein kinase, CD44, and other proteins [38]. Here, we used scratching assays to mimic damage to the RPE monolayer resulting from RPE degeneration in AMD and to study the changes in VEGF expression in RPE cells surrounding the scratched edge.

Although the scratching assay provides a view of differential VEGF expression in RPE cells around the edges, the extent of cell–cell contact loss cannot be well controlled. Accordingly, we also developed a micropatterning method to control cell–cell contact and study VEGF expression. Micropatterning techniques provide a platform to control spatial distribution of cells on various substrates and reconstruct the architecture of in vivo tissue. Micropatterning is a powerful tool for engineering the differentiation and function of cells [39,40], making in vitro tissue models [41], and studying cell–cell interactions [42]. A variety of micropatterning methods with different complexities and applications is currently available [43]. Most of these methods use cell adhesion proteins to promote cell adhesion to specific areas of substrates [44]. However, it has been shown that cell adhesion proteins can affect VEGF expression [14]. Stencil patterning, a new method of patterning, is a straightforward and reproducible alternative technique, which eliminates the need for cell adhesion proteins [45,46].

In the present study, an in vitro scratching method was used to mechanically dissociate cell–cell junctions in ARPE-19 (a human RPE cell line derived from a 19-year-old man) and human primary RPE (hRPE) cells. Both cell types are capable of expressing RPE markers [47-50]. Localized VEGF expression in scratched samples was assessed using immunocytochemistry (ICC). We also localized tight and adherens junctions in short-term (1 day after confluency) and long-term (4 weeks after confluency) RPE samples by staining N-cadherin, β-catenin, claudin-1, and ZO-1 to examine the formation of intercellular junctions. N-cadherin is the most abundant cadherin in RPE cells that mediates cell–cell adhesion at adherens junctions and modulates cellular phenotype [51-55]. Cadherins contribute to the formation of adherens junctions by associating with β-catenin [56,57]. β-catenin plays a key role in the formation of cadherin–catenin complexes through linking cadherins to α-catenin and actin fibers [58]. Claudin-1 is a member of the family of claudins and a marker of tight junctions [59,60]. ZO-1, another tight junction protein, belongs to the membrane-associated guanylate kinases (MAGUK) family [61]. VEGF phosphorylates ZO-1 and increases RPE permeability by disrupting tight junctions. Increased levels of VEGF also reduce ZO-1 expression in mesothelial, endothelial, and epithelial cells [62-66]. A recent study showed that in endothelial cells, reduced ZO-1 expression is associated with alterations in VEGF expression and cell proliferation [67].

A polydimethylsiloxane (PDMS) stencil patterning method was used to make micron-sized circular patterns (as small as 100 μm in diameter) of the ARPE-19 and hRPE cells. Growing cells on different size patterns produced varying concentrations of cells with lost junctional adhesions, allowing quantitative analysis of changes in VEGF expression. Here, using scratching assays and micropatterning techniques, we show a correlation between the loss of intercellular junctions and increased VEGF expression in RPE cells. Our findings add new insights into the mechanisms of increased VEGF expression from RPE cells during retinal degenerative diseases, such as AMD.

METHODS

Cell culture: ARPE-19 cells were obtained from American Type Culture Collections (ATCC, catalog no. CRL-2302, Manassas, VA). Cells between passages 7 and 14 were grown in standard tissue culture treated plates (Corning Inc., Corning, NY) using Dulbecco's Modified Eagle Medium/Nutrient Mixture F-12 (DMEM/F-12, Life Technologies, Carlsbad, CA) supplemented with 10% fetal bovine serum (FBS, ATCC, catalog no. 30–2020). Growth media were changed three times a week. ARPE-19 cells were grown for 4 weeks before use in the experiments. Human primary RPE cells (hRPE, Lonza, Walkersville, MD) were grown in RPE cell basal media containing supplements (RtEGM™ BulletKit, Lonza) and used until passage 4. Two percent FBS

(Lonza) was added to the media for subculturing, and the media were replaced with serum-free media after 24 h. The ARPE-19 and hRPE cells were kept in a humidified incubator at 37 °C in 5% CO_2.

Cell authentication: Short tandem repeat (STR) analysis was used to validate the ARPE-19 cells used in this study. Passage 15 was analyzed by the University of Arizona's Genetics Core's cell line authentication service. Briefly, genomic DNA was genotyped for 15 autosomal STR loci and amelogenin (X/Y) using the Promega PowerPlex 16 HS kit (Promega Corp., Madison, WI; Catalog no. DC2101). PCR was performed in an MJ Research Tetrad thermal cycler (MJ Research, Waltham, MA) using the manufacturer's recommended cycling conditions. Appropriate positive and negative controls were also amplified to ensure the accuracy of the allelic calls and to confirm that the reaction mix is free from contaminating genetic material. PCR products were separated with capillary electrophoresis using a 3730 DNA Analyzer (Applied Biosystems, Foster City, CA). The electropherograms were analyzed using GeneMarker software version 1.85 (SoftGenetics, State College, PA). Alleles were matched to the STR profile recorded with the German Collection of Microorganisms and Cell Cultures (Leibniz-Institut Deutsche Sammlung von Mikroorganismen und Zellkulturen GmbH or DSMZ). The ARPE-19 cells used in this study matched the ATCC human RPE (ARPE-19) cell line above the 80% match threshold, which is considered a match. The STR analysis results are provided in Appendix 1. The Certification of Analysis of the hRPE from Lonza is also included as passages 1–4 of the hRPE cells were used to generate the results found here. Expression of VEGF and the intercellular proteins ZO-1, N-cadherin, β-catenin, and claudin-1 by the ARPE-19 and hRPE cells (as demonstrated by the results from enzyme-linked immunosorbent assay [ELISA] and ICC) also verified the identity of the RPE cells.

Scratching assay: ARPE-19 and hRPE cells were cultured in glass-bottom well plates (Cellvis, Mountain View, CA) until a confluent monolayer formed (5–7 days). After 1 day (short-term) or 4 weeks (long-term), the monolayers were manually scratched using sterile cell scrapers (Corning Inc.) to make scratches approximately 300 µm wide. The cells were then washed twice with relevant serum-free culture media. The scratched monolayers were cultured for 24 h before immunocytochemical staining.

Micropatterning: The method used to fabricate PDMS stencils has been described previously [45,46]. Briefly, arrays of micropillars with diameters of 100, 200, and 300 µm were fabricated using SU-8 2100 photoresist (MicroChem, Corp., Newton, MA, Figure 1A). The space between the micropillars was 1 mm for all pattern sizes. The PDMS prepolymer (Sylgard 184, Dow Corning, Midland, MI) was prepared by mixing the elastomeric base and curing agent at a 10:1 v/v ratio, spun on silicon wafers containing the patterns at 1000 rpm using a CEE® model 200X spin coater, and cured at 85 °C for at least 2 h (Figure 1B). The cured PDMS membranes with through holes were peeled off the silicon wafers using wide-tip tweezers (Figure 1C). A scanning electron microscope (SEM, Quanta FEG 650 model; FEI, Hillsboro, OR) was used to examine the PDMS stencils. After the stencils were washed in ethanol, they were placed on cleaned 12 mm circular glass coverslips. The coverslips with the PDMS stencils were heat sterilized in an oven for at least 2 h at 90 °C and transferred to untreated 24-well plates (Corning Inc.). Fresh growth media (1 ml) were transferred to the wells containing the coverslips, and the well plate was degassed in a vacuum chamber for 1 h to remove air bubbles from the holes of the PDMS stencil. Vacuum degassing is essential for achieving consistent patterning of the whole coverslip surface. Treating the PDMS stencils with O_2 plasma also facilitates the removal of air bubbles. Next, 1 ml of cells at a density of 10^6 cells/ml was seeded on the PDMS stencils to cover the bottom of all through holes in PDMS with ARPE-19 or hRPE cells (Figure 1D). Cells were grown on stenciled coverslips until confluency (Figure 1E). One day after confluency, the PDMS stencils were removed, and the coverslips were gently washed twice with fresh growth media (Figure 1F). The patterned coverslips were then transferred to a new 24-well plate with the wells previously filled with 1 ml of fresh growth media and incubated until further analyses. The viability of the micropatterned cells was quantified using the Trypan blue exclusion assay (Gibco, Logan, UT). Cell counts were performed based on the nuclear counts. The nuclei were stained with NucBlue® live cell stain (Thermo Fisher Scientific, Eugene, OR; catalog no. R37605), and ImageJ software was used to facilitate counting of the nuclei. The concentration of cells with a free edge was calculated for individual cell patches as the ratio of the number of cells on the periphery of the cell patch (counted based on nuclear staining and bright-field images) over the total cell count for that patch of cells.

ELISA: Spent media from cultures of ARPE-19 and hRPE cells were collected after 24 h of growth and assayed for VEGF expression using a human VEGF ELISA kit (Life Technologies, catalog no. KHG0112). This kit measures the levels of the $VEGF_{165}$ isoform. Absorbance at 450 nm was measured using a BioTek Synergy 2 plate reader (BioTek, Winooski, VT).

Immunocytochemical staining: Extracellular VEGF expression in the patterned and scratched cultures of the ARPE-19 and hRPE cells was assessed using ICC. VEGF, ZO-1, N-cadherin, β-catenin, and claudin-1 were stained with conjugated primary monoclonal antibodies against VEGF (Novus Biologicals, Littleton, CO), ZO-1 (Thermo Fisher Scientific), N-cadherin (Novus Biologicals), β-catenin (Novus Biologicals), and claudin-1 (Thermo Fisher Scientific) at 1:100 dilution according to the manufacturer's instructions. The nuclei were counterstained with NucBlue® live cell stain. Immunostained samples were imaged using an LSM-710 Carl Zeiss (Jena, Germany) confocal microscope. Cells were grown on porous cell culture inserts (Costar Scientific Corp., Cambridge, MA) before confocal Z-stack scanning of the long-term cultures was performed. Net signal intensity graphs for VEGF were calculated over the length of the confocal images for the scratched samples using Zen 2 software (Carl Zeiss). A ridge detection plugin [68] for ImageJ software was used to calculate the total length of the cell–cell junctions and the length of the junctions covered with junctional proteins in the confocal images. The percentage of junctions covered with junctional proteins was calculated as the ratio of the length of the lines in the confocal images for relevant junctional proteins over the total length of the junctions.

Statistical analysis: Data are presented as the mean ± standard deviation. Statistical significance was determined using a Student's *t* test with $p<0.05$ indicating a statistically significant difference. Sample sizes are indicated in each figure and table.

RESULTS

The effect of losing RPE–RPE adhesion on VEGF expression was first investigated using scratching assays and ICC. ARPE-19 and hRPE cells were grown for 4 weeks (long-term) after they had reached confluency and then scratched using a cell scraper. One day after scratching, the cells were stained with anti-human VEGF antibody, and the nuclei were counterstained with 4',6-diamidino-2-phenylindole (DAPI; Figure 2). In addition, ICC was performed on the scratched cultures of the ARPE-19 and hRPE cells that had been grown for only 1 day after they reached confluency (short-term cultures). Confocal imaging of the scratched samples showed that disrupting RPE–RPE contact amplified

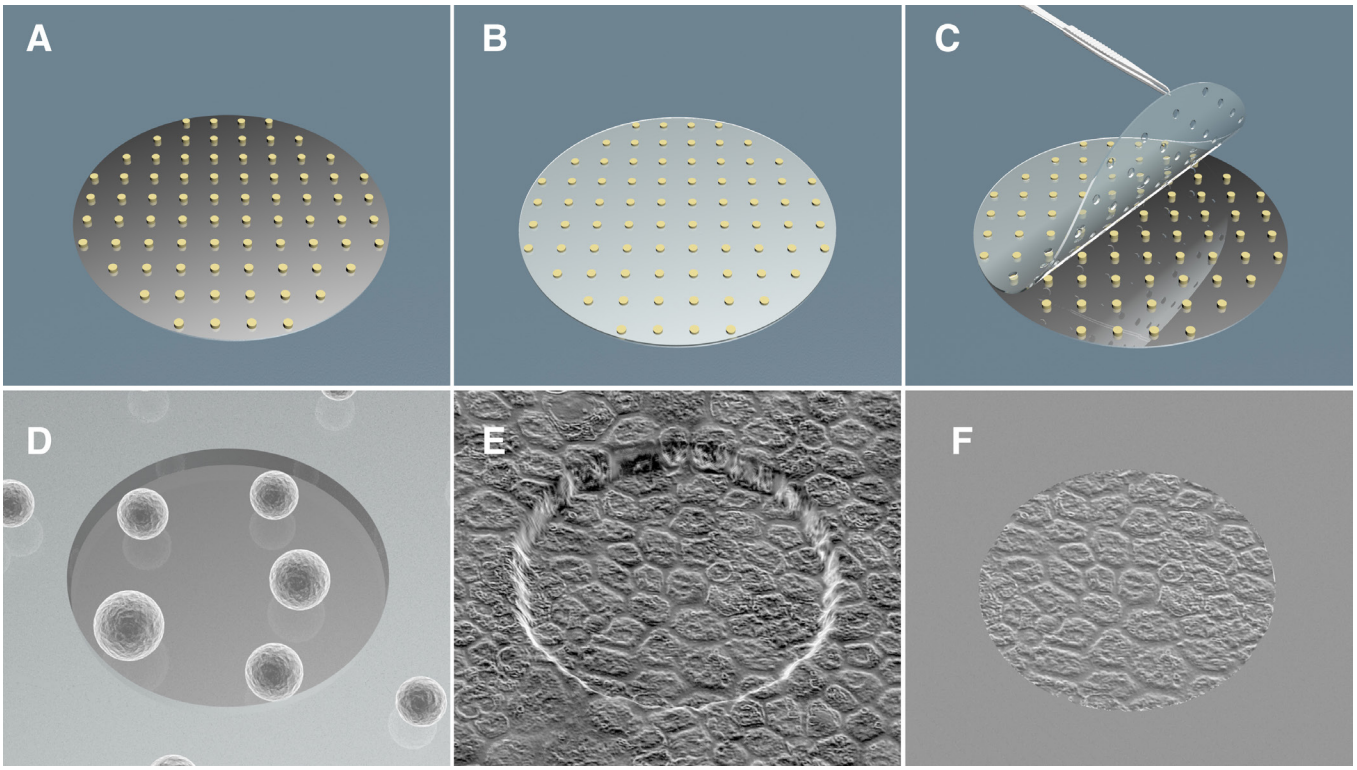

Figure 1. Schematic of PDMS stencil fabrication and micropatterning. **A**: Microfabricated photoresist pillars on a silicon wafer. **B**: Polydimethylsiloxane (PDMS) prepolymer spun on a silicon wafer with photoresist patterns. **C**: Peeling the cured PDMS stencil off the silicon wafer. **D**: Illustration of cell seeding on the stenciled coverslips. **E**: Representative schematic of the formation of the RPE monolayer. **F**: Characteristic circular pattern of the RPE cells after the PDMS stencil is peeled off the coverslip.

VEGF expression in the cells on the edges of the scratched areas in the short- and long-term RPE cultures (Figure 2). In the confocal images, a marked decrease in the net signal intensity for VEGF was observed from the scratch edge toward the middle of the monolayer in all scratched samples (Figures 2D,H,L,P). VEGF intensity was also averaged over two intensity bins at 0–100 µm and 100–200 µm from the scratch edge. For the ARPE-19 and hRPE scratch samples, the average signal intensity of the VEGF channel was higher in the 0–100 µm distance. To visualize the formation of the intercellular junctions, we used ICC to stain for the tight junction components (ZO-1 and claudin-1) and the adherens junctions (N-cadherin and β-catenin) in the short- and long-term cultures of the ARPE-19 (Figure 3) and hRPE (Figure 4) cells. According to the ICC results, ZO-1, N-cadherin, β-catenin, and claudin-1 were localized to the intercellular space in the long-term cultures (n = 3). ZO-1 was present in 88 ± 5.0% of the cell–cell junctions in the ARPE-19 cells and 98 ± 2.0% of those in the hRPE cells (Table 1). High levels of junctional localization were also seen for N-cadherin (93 ± 6.0% in the ARPE-19 cultures and 69 ± 17% in the hRPE cultures), β-catenin (82 ± 8.0% in the ARPE-19 cultures and 49 ± 13 in the hRPE cultures), and claudin-1 (only 10 ± 5.0% in the ARPE-19 cultures and 53 ± 6.0% in the hRPE cultures, Table 1). In the short-term cultures (n = 3), however, only ZO-1 was junctionally localized, with 64 ± 14% and 84 ± 7.0% of the junctions covered with ZO-1 in the ARPE-19 and hRPE cultures, respectively (Table 1). The percentage of junctional coverage with claudin-1 and β-catenin in both cell types and N-cadherin in the hRPE cultures was less than 10% in the short-term cultures. In the short-term cultures of the ARPE-19 cells, only slightly more than 25% of cell junctions were covered with N-cadherin (Table 1). We also performed a confocal z-stack scan on the long-term ARPE-19 and hRPE cultures grown on the porous cell culture inserts to confirm the polarization of the RPE cells. The results showed that in the long-term ARPE-19 cultures, although ZO-1 successfully localized to the apical regions, VEGF failed to polarize properly because its expression was not localized to either side of the culture (Figure 3M). In the long-term hRPE cultures, ZO-1 was localized to apical and intercellular areas, and the expression of VEGF was mainly basolateral, confirming the polarization of cells after 4 weeks (Figure 4M).

Results of the scratching experiments followed by ZO-1 and VEGF staining showed that in the ARPE-19 and hRPE cultures, VEGF expression was higher on the edges of the cell patches, where the cell–cell contact was missing, and lower in the confluent areas of the monolayer with higher ZO-1 junctional localization. VEGF expression was inversely proportional to the localization of ZO-1 to the intercellular junctions. In other words, with less junctional localization of ZO-1, VEGF expression was higher and vice versa (Figure 5A–C).

Based on the scratching results, we hypothesized losing intercellular junctions, and therefore, reduced cell–cell interactions, may contribute to increased VEGF expression. Inducing VEGF expression from cells with a free edge in the short-term scratched cultures suggests that intercellular junctions that occur early after cell–cell contact, such as ZO-1, may be involved in VEGF regulation. To verify these results, we used a micropatterning method to quantitatively study and control the loss of cell–cell contact on VEGF expression in short-term cultures of ARPE-19 and hRPE cells.

For micropatterning, a PDMS stencil micropatterning method was used to make micropatterns of the RPE cells. The SEM images showed that the diameter of the through holes in the PDMS membranes was 102.7 ± 4.60, 213.4 ± 3.800, and 307.3 ± 10.50 µm for the 100, 200, and 300 µm patterns, respectively (n = 9; Figure 6A–C; Table 2). These membranes made consistent circular patterns of ARPE-19 and hRPE cells on the glass substrates. Figure 6D–F shows ARPE-19 cells attaching to the exposed glass in the presence of PDMS stencils. Figure 6G–I shows single patches of hRPE cells patterned on glass coverslips after the PDMS stencil was removed. Figure 7A shows that varying concentrations of cells on the periphery of the patterns could successfully be produced using this micropatterning method. The average cell patch size was 101.5 ± 4.000, 213 ± 11.0, and 311.5 ± 10.00 µm in diameter, and the average cell count per patch was approximately 6.0 ± 2.0, 28 ± 6.0, and 96 ± 16, respectively (n = 21; Table 2). Patterning on the smallest pattern size (100 µm) produced the highest concentration of peripheral cells with approximately 93% of all cells losing junctional cell–cell adhesion at least on one side. This percentage decreased to 54 and 33 for the 200 and 300 µm pattern sizes, respectively (n = 21; Figure 7A; Table 2). The size of the cell patches increased for both cell types 48 h after the stencil was removed, with this increase greater for ARPE-19 patches (Figure 7B). The viability of micropatterned ARPE-19 and hRPE cells was greater than 93% for all pattern sizes.

ICC was used to localize the expression of ZO-1 and VEGF in the micropatterned samples. The results showed that the expression of VEGF was higher on the periphery of the ARPE-19 and hRPE micropatterns. Similar to the scratched samples, this increase in VEGF expression was associated with the translocation of ZO-1 from the junctional zones (Figure 5D–I). VEGF expression in the spent media of the patterned ARPE-19 and hRPE cells was analyzed using a VEGF ELISA kit (n = 9). To quantitatively compare

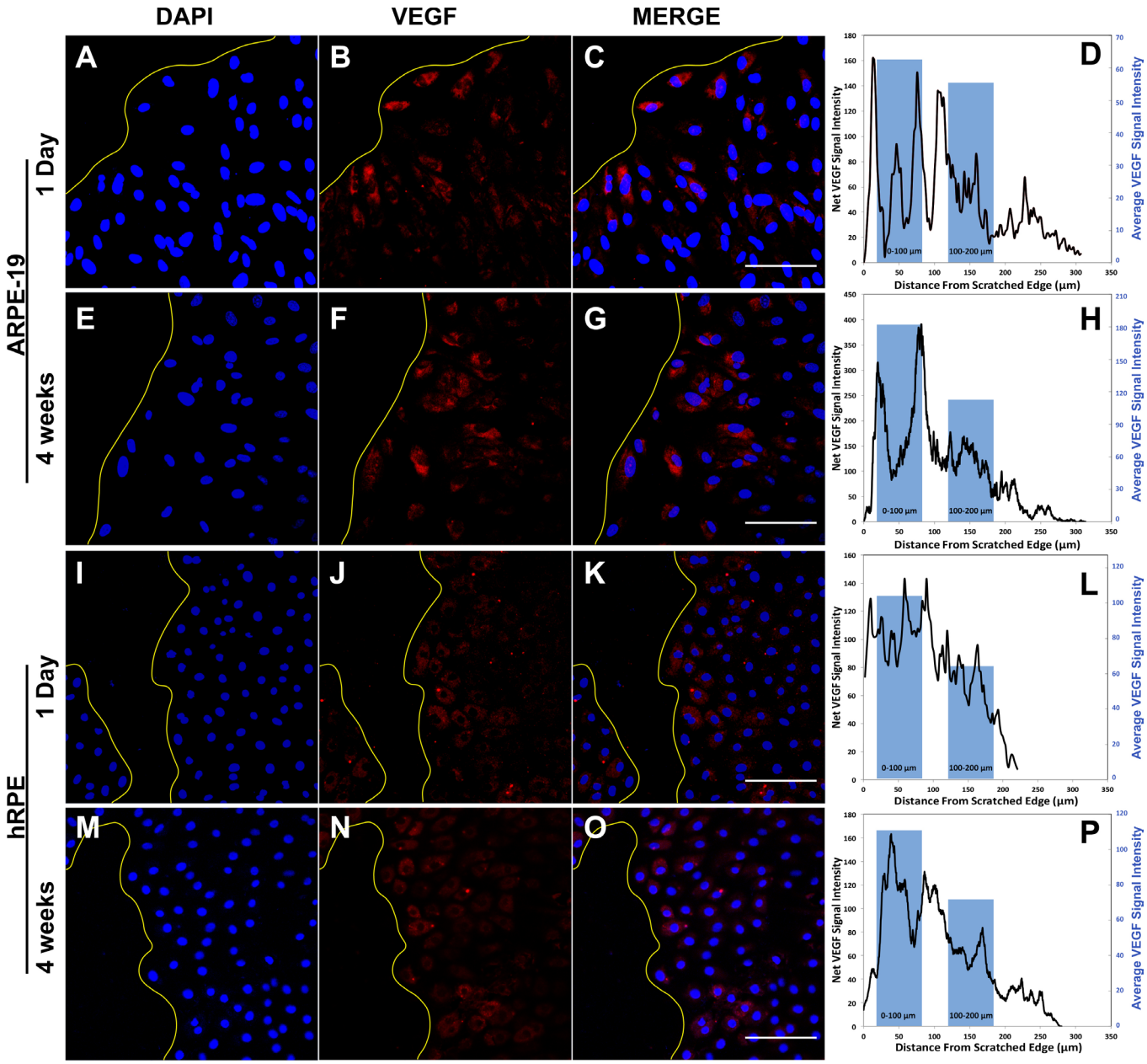

Figure 2. ICC results for scratched cultures of ARPE-19 and hRPE cells. Results show confocal images for short-term (1 day after confluency) and long-term (4 weeks after confluency) cultures of ARPE-19 (**A-C**, **E-G**) and hRPE (**I-K**, **M-O**) cells. VEGF expression was elevated along the edges of scratched areas in all sample types. Graphs **D**, **H**, **L**, and **P** show net signal intensity for VEGF along the length of the relevant confocal image (line graphs) and the average VEGF signal intensity at 0-100 µm and 100-200 µm from the scratched edge (bar graphs). The net signal intensity was higher proximal to the scratch zone and lower in confluent areas for all samples. The average signal intensity was higher in the first 100 µm from the scratch edge for all samples. Blue = 4',6-diamidino-2-phenylindole (DAPI); red = VEGF. Yellow lines indicate the scratch edge. Scale bars = 100 µm.

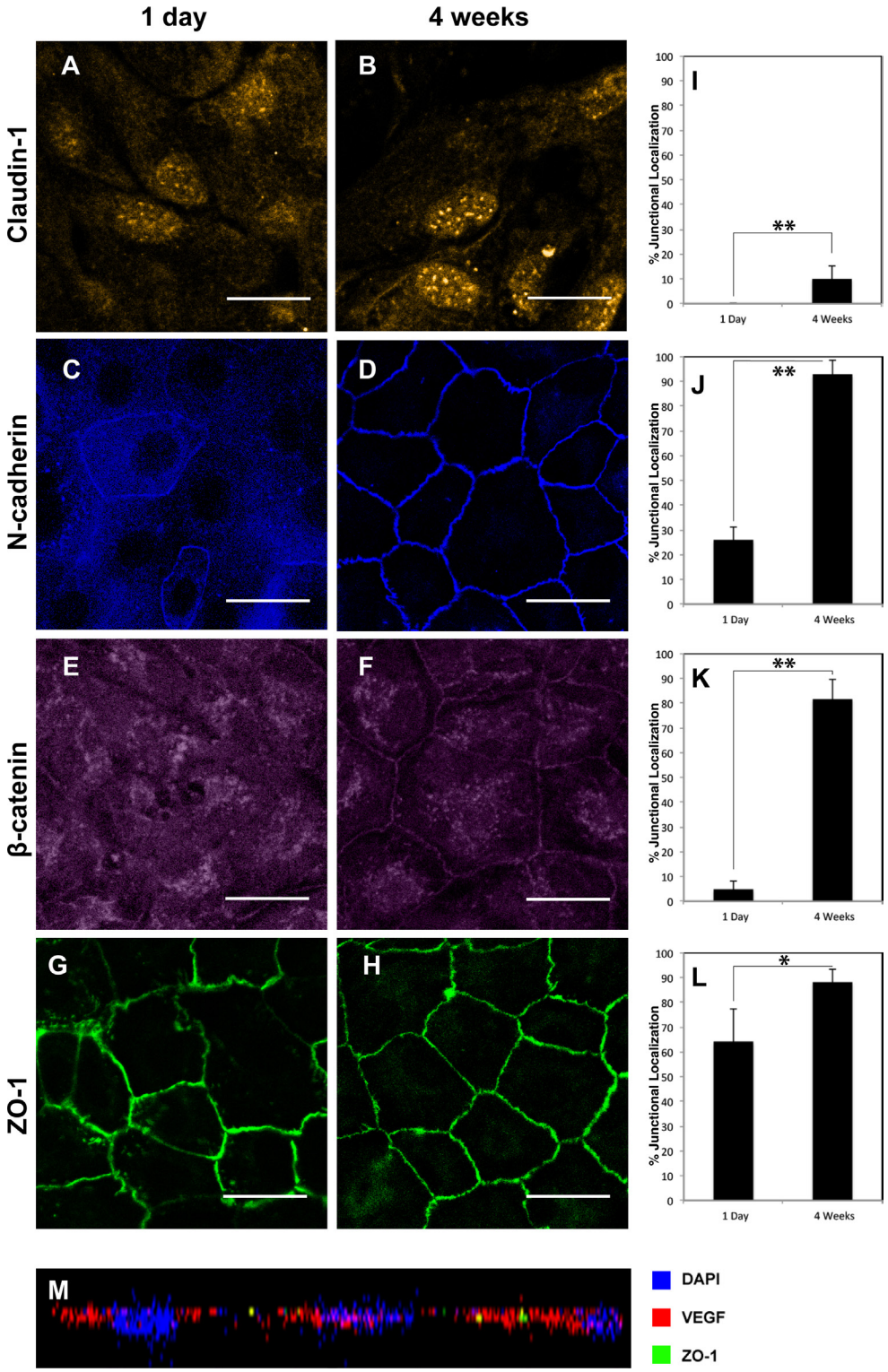

Figure 3. ICC results for confluent ARPE-19 cultures. Cells were immunostained for Claudin-1 (**A**, **B**), N-cadherin (**C**, **D**), β-catenin (**E**, **F**) and ZO-1 (**G**, **H**). **I**-**L**: Percentage of intercellular junctions covered by the corresponding protein in cultures of ARPE-19 cells grown for 1 day or 4 weeks after reaching confluency. All junctional proteins, except for ZO-1, had limited localization after 1 day at confluence. In all cases, junctional localization increased significantly after 4 weeks. Data represent the mean ± standard deviation for three replicates from three representative confocal images per each time point for each junctional protein (n = 3). * $p<0.05$, ** $p<0.01$. **M**: Z-stack scan for a long-term (4 weeks after confluency) of ARPE-19 cells grown on porous cell culture inserts. ZO-1 was localized to the apical junctional areas, while VEGF failed to polarize. Scale bar = 25 µm.

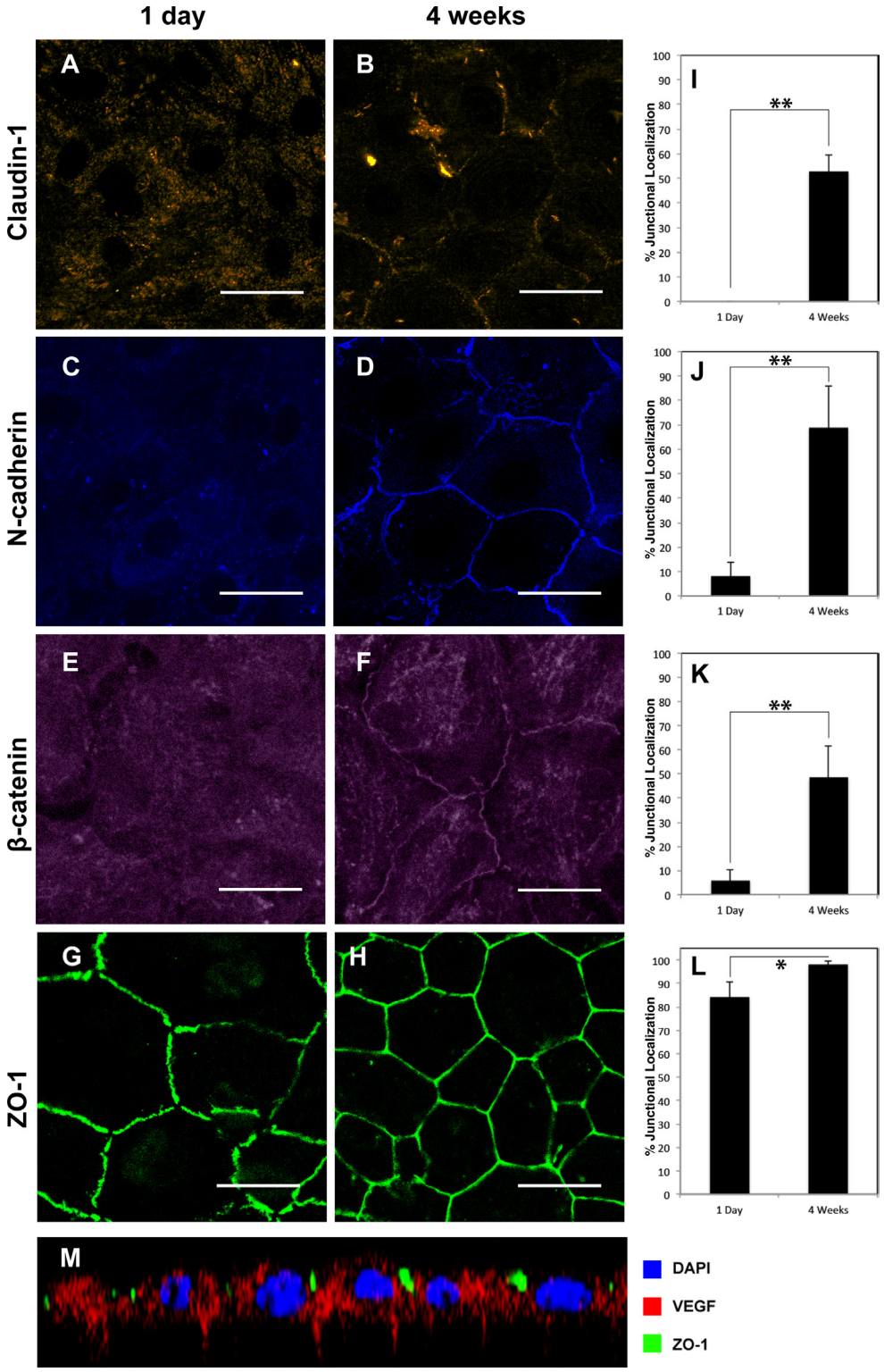

Figure 4. ICC results for confluent hRPE cultures. Cells were immunostained for Claudin-1 (**A**, **B**), N-cadherin (**C**, **D**), β-catenin (**E**, **F**) and ZO-1 (**G**, **H**). **I**-**L**: Percentage of intercellular junctions covered by the corresponding protein in cultures of hRPE cells grown for 1 day or 4 weeks after reaching confluency. All junctional proteins, except for ZO-1, had limited localization after 1 day post confluence. In all cases, junctional localization increased markedly after 4 weeks. Data represent the mean ± standard deviation for three replicates from three representative confocal images per each time point for each junctional protein (n = 3). * $p<0.05$, ** $p<0.01$. **M**. Z-Stack scan for a long-term (4 weeks after confluency) culture of hRPE cells grown on porous cell culture inserts, confirming apical localization of ZO-1 and basolateral localization of VEGF. Scale bar = 25 µm.

Table 1. Percentage of cell-cell junctions covered with junctional proteins, Claudin-1, N-cadherin, catenin and ZO-1, in short-term (1 day after confluence) and long-term (4 weeks after confluence) cultures of ARPE-19 and hRPE cells.

Cell type	Time after confluence	Cell-cell junctions covered with junctional protein (%)			
		Claudin-1	N-cadherin	β-catenin	ZO-1
ARPE-19	1 Day	0	26±5	5±3	64±14
	4 Weeks	10±5	93±6	82±8	88±5
hRPE	1 Day	0	8±6	6±5	84±7
	4 Weeks	53±6	69±17	49±13	98±2

Data represent the mean ± standard deviation for 3 replicates (3 representative confocal images for each junctional protein and each time point; n = 3).

VEGF expression in cells grown on different pattern sizes, specific VEGF expression was calculated by dividing the total VEGF measured in the spent media after 24 h by the total number of cells (VEGF/ml.cell). With smaller pattern sizes, increasing levels of VEGF expression were observed from the ARPE-19 and hRPE cells (Figure 7C,D). To further investigate the effect of the patch size, the cells were grown for another 24 h in fresh media before the spent media were analyzed for VEGF expression. Specific VEGF expression slightly decreased at day 2. This change in VEGF expression at day 2 was greater in the ARPE-19 patterns (Figure 7C,D).

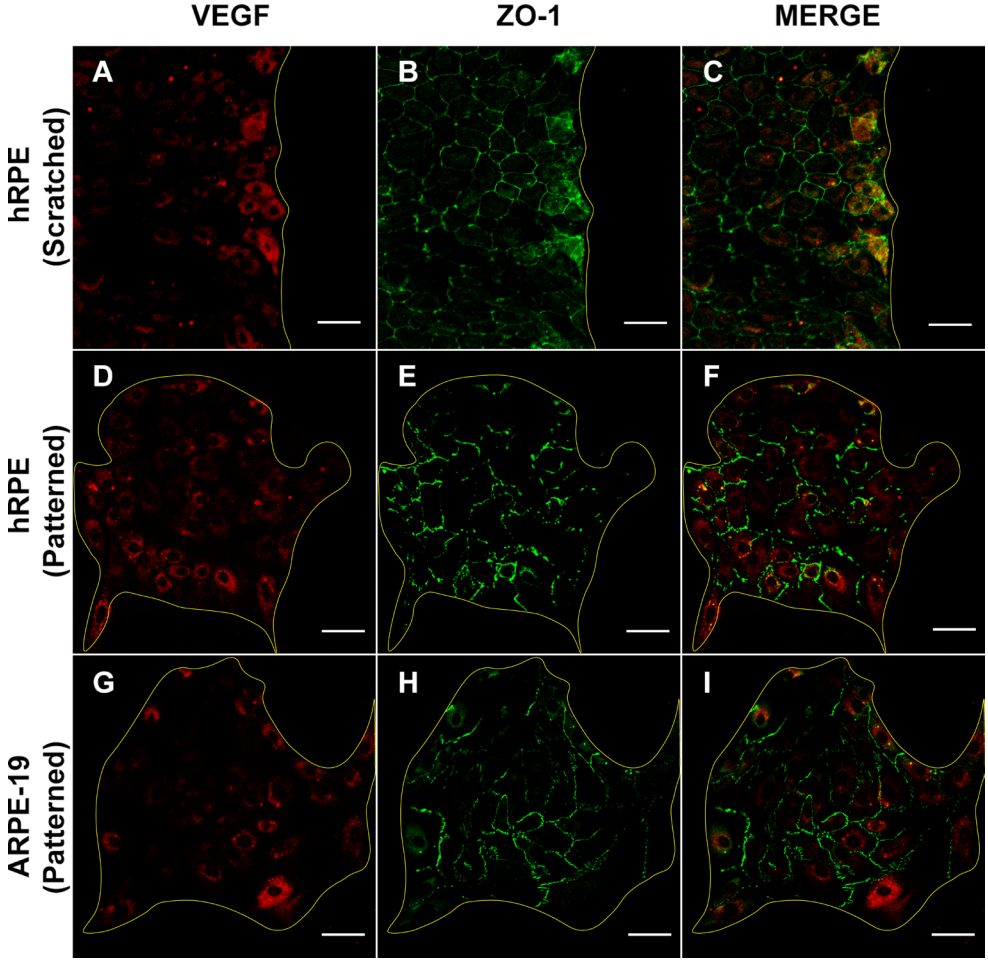

Figure 5. Confocal ICC images of scratched and micropatterned RPE cultures. ZO-1 and VEGF were immunostained in a long-term hRPE culture (4 weeks after confluency) 24 h after scratching (**A**-**C**) and micropatterned hRPE (**D**-**F**) and ARPE-19 cells (**G**-**I**) 24 hours after removing PDMS stencils. VEGF expression increased in cells proximal to the scratched area (**A**) and along the periphery of the micropatterns (**D**, **G**). This increase in VEGF expression correlated with dislocalization of ZO-1 from intercellular zones to the cytoplasm in both scratched and micropatterned samples (**B**, **E**, **H**). Red = VEGF; green = ZO-1. Yellow lines indicate the scratch edge (**A**-**C**) and micropattern edges (**D**-**I**). Scale bar = 50 µm.

DISCUSSION

Although there is a large body of evidence linking increased VEGF expression in the RPE to pathologic neovascularization of the retina [3-10], the exact mechanisms leading to the imbalance of VEGF in wet AMD are not fully understood. The failure of RPE–RPE adhesion is known as a consequence of neovascularization but is not usually considered a mechanism that contributes to the pathogenesis of CNV. The present study demonstrates that losing RPE–RPE attachment can induce VEGF overexpression and that early cell–cell contact can regulate VEGF expression.

Scratching and micropatterning methods were developed to study the role of junctional RPE adhesion on VEGF expression. In particular, immunostaining the scratched samples for VEGF showed a higher level of VEGF in cells with lost junctional adhesion mainly on the edges of the RPE cell monolayers (Figure 2), suggesting a regulatory role for RPE cell–cell adhesion in VEGF expression. Junctional localization of claudin-1, N-cadherin, β-catenin, and ZO-1 in long-term hRPE cultures and the polarization of VEGF and ZO-1 expression demonstrated the proper formation of the intercellular junctions and the maturity of the hRPE cells. Despite the lack of proper polarization of ARPE-19 cells in the long-term cultures, the effect of losing cell–cell adhesion on VEGF expression in the ARPE-19 cells was similar to that in the hRPE cells. Aberrant localization of VEGF in ARPE-19 cells has previously been observed [50,69]. Here, we found that overexpression of VEGF occurs in short-term cultures, implying that early contact between neighboring

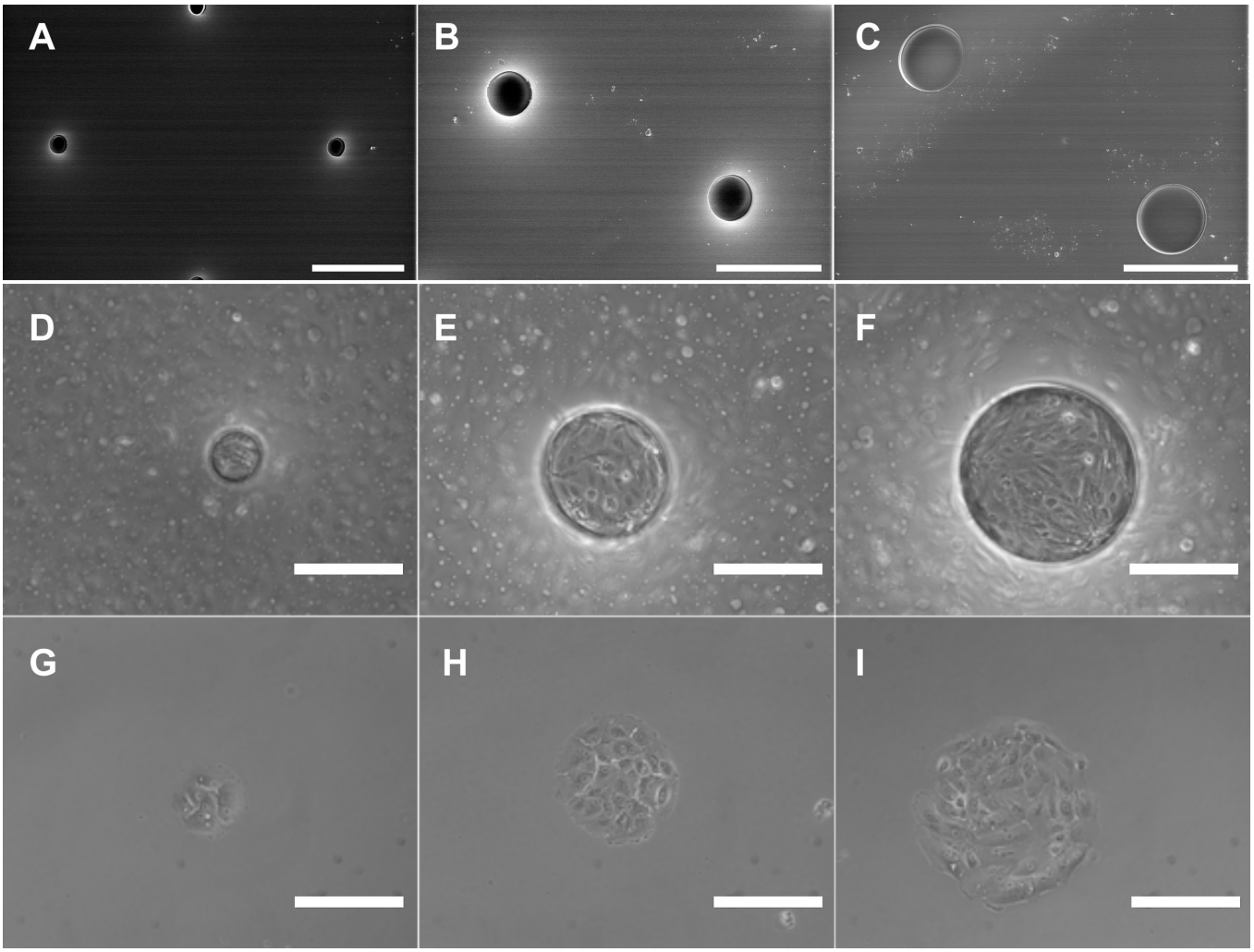

Figure 6. Micropatterning of ARPE-19 and hRPE cells. **A**–**C**: Scanning electron microscope (SEM) images of through holes of different sizes (**A**: 100, **B**: 200, and **C**: 300 µm in diameter) in the polydimethylsiloxane (PDMS) stencils. The lateral spacing between the holes was 1 mm for all pattern sizes. **D**–**F**: ARPE-19 cells attached to glass coverslips through PDMS stencil holes after 24 h. **G**–**I**: hRPE cells on glass coverslips, after the PDMS stencils were removed. Scale bars, **A**–**C** = 500 µm; **D**–**I** = 200 µm.

Table 2. Micropatterning results.

Nominal Pattern Size (µm)			100	200	300
Diameter of Through Holes in PDMS Stencils (µm)			102.7±4.6	213.4±3.8	307.3±10.5
Cell Patch Diameter (µm)	ARPE-19	Day 0	101.5±4	213±11	311.5±10
		Day 1	120.3±14	225.3±13	349.2±26
		Day 2	176.2±23	355.3±27	488.8±43
	hRPE	Day 0	101±6	210±10	308±12
		Day 1	108.8±7	217.7±12	326.2±16
		Day 2	121.8±14	240±29	369.8±44
Cell Count (Cells/Patch)	ARPE-19	Day 0	6±2	28±6	96±16
Concentration of Cells with a Free Edge (%)	ARPE-19	Day 0	93±7	54±7	33±4

Day 0 measurements taken immediately after removing the PDMS stencils. Day 1 and 2 are 1 and 2 days after removing the PDMS stencils, respectively. Data represent the mean ± standard deviation for three replicates. For the diameter of through holes in PDMS, three measurements per pattern size per replicate (n = 9) are reported. For the cell patch measurements, seven measurements per replicate (n = 21) for each pattern size and each time point are listed.

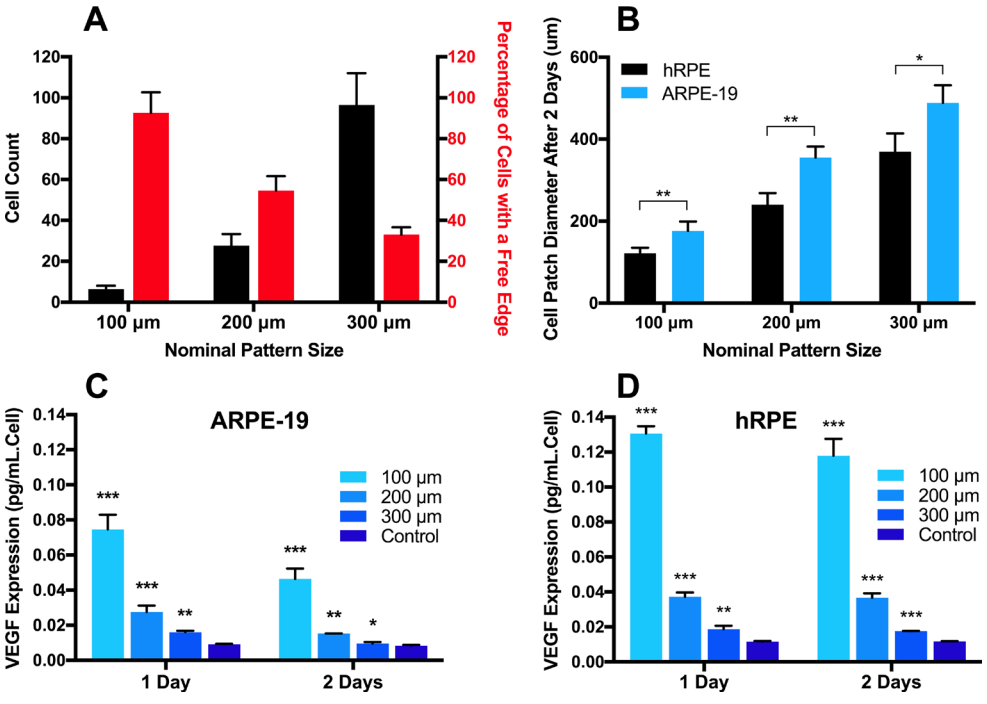

Figure 7. Micropatterning results. **A**: Formation of varying concentrations of ARPE-19 cell with a free edge by micropatterning. Black = average number of cells per cell patch of corresponding size; red = concentration of cells losing cell–cell contact at least on one side. Increase in the concentration of cells losing cell–cell contact correlates negatively with cell count and patch size. Data represent the mean ± standard deviation for three replicates (seven measurements per replicate for each pattern size and each time point; n = 21). Similar results were seen for the human RPE (hRPE) cells (data not shown). **B**: Increase in the cell patch diameter at day 2. A greater increase in patch diameter was observed for the ARPE-19 cells compared with the hRPE cells. Data represent the mean ± standard deviation for three replicates (seven measurements per replicate for each pattern size and each time point; n = 21). **C**, **D**: VEGF expression analysis with enzyme-linked immunosorbent assay (ELISA) for the micropatterned ARPE-19 (**C**) and hRPE (**D**) cells. VEGF expression is presented as the total VEGF divided by the cell count. The smaller the pattern size, the higher the VEGF expression per cell. VEGF expression decreased during day 2 presumably because of the increased pattern sizes due to cell growth (**B**). Data represent the mean ± standard deviation for three replicates (three measurements per replicate for each pattern size and each time point; n = 9); * p<0.05, ** p<0.01, *** p<0.001. P values are relative to the control (confluent) samples.

cells is a key step in VEGF regulation. Therefore, it is likely that early-forming junctional complexes have a role in regulating VEGF expression.

Figure 2 shows that VEGF is induced in the RPE cells at the edges of the scratched areas. According to the ICC results (Figure 3 and Figure 4), ZO-1 is one of the first junctional proteins to localize to intercellular zones. Figure 5 shows that the delocalization of ZO-1 correlates strongly to increased VEGF expression in the scratched zones and along the periphery of the micropatterns. ZO-1 is an important component of intercellular signal transduction in epithelial and endothelial cells [70,71]. Previous studies have implicated VEGF in the phosphorylation and delocalization of ZO-1 [66,72]. A recent study showed that changes in ZO-1 expression can affect VEGF expression in endothelial cells [67]. Moreover, aberrant angiogenesis has been reported in the yolk sac of ZO-1-deficient mice [73]. In RPE cells, inhibiting ZO-1 expression induces proliferation. More effort is needed to clarify whether ZO-1 or other junctional proteins that contribute to early stages of junction formation can regulate VEGF expression in RPE cells. Nevertheless, our results show a clear relationship between the loss of junctional RPE cell adhesion and VEGF expression.

To quantitatively evaluate the hypothesis that the observed increase in VEGF expression is due, at least in part, to reduced cell–cell contact, we produced varying concentrations of cells with reduced cell–cell contact by growing RPE cells on different pattern sizes (Table 2; Figure 7A) using micropatterning. One advantage of the physical detachment of cells by micropatterning compared with chemical methods, such as calcium-mediated dissociation, is that it eliminates any possible side effect on VEGF expression from the chemicals typically used for dissociating cellular junctions [74]. By using PDMS stencils, we also eliminated the need for cell adhesion proteins, which may affect VEGF expression [14]. The quantitative ELISA results from the micropatterning experiments confirmed our hypothesis that losing cell–cell adhesion increases VEGF expression (Figure 7C,D). These findings confirm previous observations from calcium-mediated RPE dissociation studies [32,33]. In the patterning experiments, the ARPE-19 cells behaved similarly to the hRPE cells in terms of VEGF expression. The VEGF expression from ARPE-19 cells was only slightly lower than that of the hRPE cells. The decreased VEGF expression at day 2 of patterning, observed for both cell types, is presumably due to cell growth leading to an increase in patch size and consequently the decreased concentration of the cells on the edges of the patterns. This change in VEGF expression at day 2 decreased to a greater extent in the ARPE-19 cells than in the hRPE cells, potentially due to the shorter doubling time of the ARPE-19 cells compared with that of the hRPE cells, leading to faster growth of the size of the cell patches (Figure 7B–D).

During the latest stages of dry AMD, the loss of physical contact between RPE cells occurs due to RPE cell death in GA [29-31]. In a study on patients with AMD with GA, CNV started at the peripheral borders of the atrophic sites in nearly 70% of the eyes that developed CNV, implying that cell–cell contact may have a role in the progression of dry AMD to wet AMD [75]. RPE cells may also physically detach from each other because of breaks (tears) in the RPE monolayer. RPE tears occur spontaneously secondary to neovascular AMD or after intravitreal injection of antiangiogenic drugs [20-28]. The present findings suggest that physical perturbations in the RPE, which may result from RPE degeneration, RPE tears, drusen formation, or apoptosis associated with aging, can induce the initiation and/or progression of CNV due to the overexpression of VEGF. Particularly, our results are consistent with a previous finding that the expression of VEGF isoforms was markedly increased in the RPE cells along the edges of a surgically removed subretinal vascular membrane of a patient with AMD [33]. The present results may also explain observations that CNV is associated with the surviving RPE cells in atrophic areas of retinas with AMD [76]. It is possible that this association of CNV with surviving RPE cells may be a consequence of tight junction loss and increased VEGF expression in and from RPE cells at atrophic sites. Given that CNV occurs during the latest stages of AMD, it may be possible to prevent CNV by implementing anti-VEGF therapies earlier, as soon as defects in RPE–RPE integrity are detected. Moreover, the present findings suggest that anti-VEGF therapies may be required even after the development of RPE tears to prevent excessive VEGF expression due to the loss of cell–cell contact in the RPE.

The ELISA kit used here can quantify the levels of $VEGF_{165}$. This isoform is the most potent and most abundant VEGF isoform in the RPE [77,78]. Nevertheless, further research is needed to study the effect of losing cell–cell contact on the expression of other isoforms of VEGF, such as $VEGF_{121}$, and to identify the association between RPE cell–cell signaling and VEGF overexpression in wet AMD. Work in this direction is ongoing in our laboratory.

Conclusions: Increasing the loss of cell–cell contact induced VEGF protein expression in ARPE-19 and hRPE cells. In addition, we demonstrated that there is a correlation between the loss of intercellular junctions and increased VEGF expression.

APPENDIX 1. STR ANALYSIS.

To access the data, click or select the words "Appendix 1."

ACKNOWLEDGMENTS

The authors thank Lori Caldwell for assistance with SEM imaging and Cynthia Hanson, Charles Harding, and Kara Swenson for their assistance in editing. This work was supported by a Career Starter Grant from the Knights Templar Eye Foundation and a Ralph E. Powe Junior Faculty Award from the Oak Ridge Associated Universities (ORAU). We acknowledge support from the Microscopy Core Facility at Utah State University for the SEM images. The facility maintains an SEM acquired through a National Science Foundation Major Research Instrumentation grant (CMMI-1337932).

REFERENCES

1. Ferris FL, Fine SL, Hyman L. Age-related macular degeneration and blindness due to neovascular maculopathy. Arch Ophthalmol Chic Ill 1960; 1984:1640-2. [PMID: 6208888].
2. Das A, McGuire PG. Retinal and choroidal angiogenesis: pathophysiology and strategies for inhibition. Prog Retin Eye Res 2003; 22:721-48. [PMID: 14575722].
3. Hera R, Keramidas M, Peoc'h M, Mouillon M, Romanet J-P, Feige J-J. Expression of VEGF and angiopoietins in subfoveal membranes from patients with age-related macular degeneration. Am J Ophthalmol 2005; 139:589-96. [PMID: 15808152].
4. Spilsbury K, Garrett KL, Shen W-Y, Constable IJ, Rakoczy PE. Overexpression of Vascular Endothelial Growth Factor (VEGF) in the Retinal Pigment Epithelium Leads to the Development of Choroidal Neovascularization. Am J Pathol 2000; 157:135-44. [PMID: 10880384].
5. Baffi J, Byrnes G, Chan C-C, Csaky KG. Choroidal Neovascularization in the Rat Induced by Adenovirus Mediated Expression of Vascular Endothelial Growth Factor. Invest Ophthalmol Vis Sci 2000; 41:3582-9. [PMID: 11006256].
6. Heier JS, Antoszyk AN, Pavan PR, Leff SR, Rosenfeld PJ, Ciulla TA, Dreyer RF, Gentile RC, Sy JP, Hantsbarger G, Shams N. Ranibizumab for Treatment of Neovascular Age-Related Macular Degeneration: A Phase I/II Multicenter, Controlled, Multidose Study. Ophthalmology 2006; 113:633-642.e4. [PMID: 16483659].
7. Rosenfeld PJ, Brown DM, Heier JS, Boyer DS, Kaiser PK, Chung CY, Kim RY. Ranibizumab for Neovascular Age-Related Macular Degeneration. N Engl J Med 2006; 355:1419-31. [PMID: 17021318].
8. Saishin Y, Saishin Y, Takahashi K, Silva RL, Hylton D, Rudge JS, Wiegand SJ. Campochiaro PA. VEGF-TRAPR1R2 suppresses choroidal neovascularization and VEGF-induced breakdown of the blood–retinal barrier. J Cell Physiol 2003; 195:241-8. [PMID: 12652651].
9. Krzystolik MG, Afshari MA, Adamis AP, Gaudreault J, Gragoudas ES, Michaud NA, Li W, Connolly E, O'Neill CA, Miller JW. Prevention of experimental choroidal neovascularization with intravitreal anti-vascular endothelial growth factor antibody fragment. Arch Ophthalmol Chic Ill. 2002; 120:338-46. [PMID: 11879138].
10. Rosenfeld PJ, Villate N, Feuer WJ, Puliafito CA, McCluskey ER. RhuFab V2 (Anti-VEGF Antibody Fragment) in Neovascular AMD: Safety, Tolerability, and Efficacy of Multiple, Escalating Dose Intravitreal Injections. Invest Ophthalmol Vis Sci 2003; 44:970-970. .
11. Ford KM, Saint-Geniez M, Walshe T, Zahr A, D'Amore PA. Expression and Role of VEGF in the Adult Retinal Pigment Epithelium. Invest Ophthalmol Vis Sci 2011; 52:9478-87. [PMID: 22058334].
12. Saint-Geniez M, Maldonado AE, D'Amore PA. VEGF Expression and Receptor Activation in the Choroid during Development and in the Adult. Investig Opthalmology Vis Sci. 2006; 47:3135-[PMID: 16799060].
13. Shima DT, Deutsch U, D'Amore PA. Hypoxic induction of vascular endothelial growth factor (VEGF) in human epithelial cells is mediated by increases in mRNA stability. FEBS Lett 1995; 370:203-8. [PMID: 7656977].
14. Mousa SA, Lorelli W, Campochiaro PA. Role of hypoxia and extracellular matrix-integrin binding in the modulation of angiogenic growth factors secretion by retinal pigmented epithelial cells. J Cell Biochem 1999; 74:135-43. [PMID: 10381270].
15. Vinores SA, Xiao W-H, Aslam S, Shen J, Oshima Y, Nambu H, Liu H, Carmeliet P, Campochiaro PA. Implication of the hypoxia response element of the vegf promoter in mouse models of retinal and choroidal neovascularization, but not retinal vascular development. J Cell Physiol 2006; 206:749-58. [PMID: 16245301].
16. Zhang P, Wang Y, Hui Y, Hu D, Wang H, Zhou J, Du H. Inhibition of VEGF Expression by Targeting HIF-1α with Small Interference RNA in Human RPE Cells. Ophthalmologica 2007; 221:411-7. [PMID: 17947829].
17. Nagineni CN, Kommineni VK, William A, Detrick B, Hooks JJ. Regulation of VEGF expression in human retinal cells by cytokines: Implications for the role of inflammation in age-related macular degeneration. J Cell Physiol 2012; 227:116-26. [PMID: 21374591].
18. Nozaki M, Raisler BJ, Sakurai E, Sarma JV, Barnum SR, Lambris JD, Chen Y, Zhang K, Ambati BK, Baffi JZ, Ambati J. Drusen complement components C3a and C5a promote choroidal neovascularization. Proc Natl Acad Sci USA 2006; 103:2328-33. [PMID: 16452172].
19. Yoshida T. The potential role of amyloid in the pathogenesis of age-related macular degeneration. J Clin Invest 2005; 115:2793-800. [PMID: 16167083].
20. Hoskin A, Bird AC, Sehmi K. Tears of detached retinal pigment epithelium. Br J Ophthalmol 1981; 65:417-22. [PMID: 7260013].

21. Yeo JH, Marcus S, Murphy RP. Retinal pigment epithelial tears. Patterns and prognosis. Ophthalmology 1988; 95:8-13. [PMID: 2449643].

22. Pauleikhoff D, Löffert D, Spital G, Radermacher M, Dohrmann J, Lommatzsch A, Bird A. Pigment epithelial detachment in the elderly. Graefes Arch Clin Exp Ophthalmol 2002; 240:533-8. [PMID: 12136282].

23. Pece A, Vitale L, Milani P, Pierro L. Spontaneous reattachment of the margins of a macular retinal pigment epithelium tear: optical coherence tomography documentation of a case. Ophthalmol J Int Ophtalmol Int J Ophthalmol Z Augenheilkd. 2010; 224:159-61. [PMID: 19752583].

24. Leon PE, Saviano S, Zanei A, Pastore MR, Guaglione E, Mangogna A, Tognetto D. Spontaneous or secondary to intravitreal injections of anti-angiogenic agents retinal pigment epithelial tears in age-related macular degeneration. Int J Ophthalmol 2014; 7:681-5. [PMID: 25161943].

25. Bakri SJ, Patel SP. Retinal pigment epithelial tear following intravitreal bevacizumab. Eye (Lond) 2006; 21:424-5. [PMID: 17187026].

26. Shah CP, Hsu J, Garg SJ, Fischer DH, Kaiser R. Retinal Pigment Epithelial Tear After Intravitreal Bevacizumab Injection. Am J Ophthalmol 2006; 142:1070-1071.e1. [PMID: 17157598].

27. Bakri SJ, Kitzmann AS. Retinal Pigment Epithelial Tear after Intravitreal Ranibizumab. Am J Ophthalmol 2007; 143:505-7. [PMID: 17317396].

28. Konstantinidis L, Ambresin A, Zografos L, Mantel I. Retinal pigment epithelium tears after intravitreal injection of ranibizumab for predominantly classic neovascular membranes secondary to age-related macular degeneration. Acta Ophthalmol (Copenh) 2010; 88:736-41. [PMID: 19604160].

29. Dunaief JL, Dentchev T, Ying G-S, Milam AH. The Role of Apoptosis in Age-Related Macular Degeneration. Arch Ophthalmol 2002; 120:1435-42. [PMID: 12427055].

30. Hanus J, Zhang H, Wang Z, Liu Q, Zhou Q, Wang S. Induction of necrotic cell death by oxidative stress in retinal pigment epithelial cells. Cell Death Dis 2013; 4:e965-[PMID: 24336085].

31. Liang F-Q, Godley BF. Oxidative stress-induced mitochondrial DNA damage in human retinal pigment epithelial cells: a possible mechanism for RPE aging and age-related macular degeneration. Exp Eye Res 2003; 76:397-403. [PMID: 12634104].

32. Wang X-F, Cui JZ, Prasad SS, Matsubara JA. Altered Gene Expression of Angiogenic Factors Induced by Calcium-Mediated Dissociation of Retinal Pigment Epithelial Cells. Investig Opthalmology Vis Sci. 2005; 46:1508-[PMID: 15790923].

33. Ikeda Y, Yonemitsu Y, Onimaru M, Nakano T, Miyazaki M, Kohno R, Nakagawa K, Ueno A, Sueishi K, Ishibashi T. The regulation of vascular endothelial growth factors (VEGF-A, -C, and -D) expression in the retinal pigment epithelium. Exp Eye Res 2006; 83:1031-40. [PMID: 16842779].

34. Cheng H-C, Ho T-C, Chen S-L, Lai H-Y, Hong K-F, Tsao Y-P. Troglitazone suppresses transforming growth factor beta-mediated fibrogenesis in retinal pigment epithelial cells. Mol Vis 2008; 14:95-104. [PMID: 18253093].

35. Qiu S, Jiang Z, Huang Z, Chen X, Qian X, Gao Q, Zheng H. Migration of Retinal Pigment Epithelium Cells Is Regulated by Protein Kinase Cα In VitroMigration of RPE Cells Is Regulated by PKCα In Vitro. Invest Ophthalmol Vis Sci 2013; 54:7082-90. [PMID: 24084091].

36. Sugino IK, Wang H, Zarbin MA. Age-related macular degeneration and retinal pigment epithelium wound healing. Mol Neurobiol 2003; 28:177-94. [PMID: 14576455].

37. Campochiaro PA, Hackett SF, Vinores SA, Freund J, Csaky C, LaRochelle W, Henderer J, Johnson M, Rodriguez IR, Friedman Z. Platelet-derived growth factor is an autocrine growth stimulator in retinal pigmented epithelial cells. J Cell Sci 1994; 107:2459-69. [PMID: 7844163].

38. Singh S, Zheng JJ, Peiper SC, Mclaughlin BJ. Gene expression profile of ARPE-19 during repair of the monolayer. Graefes Arch Clin Exp Ophthalmol Albrecht Von Graefes Arch Klin Exp Ophthalmol. 2001; 239:946-51. [PMID: 11820701].

39. Tang J, Peng R, Ding J. The regulation of stem cell differentiation by cell-cell contact on micropatterned material surfaces. Biomaterials 2010; 31:2470-6. [PMID: 20022630].

40. Singhvi R, Kumar A, Lopez GP, Stephanopoulos GN, Wang DI, Whitesides GM, Ingber DE. Engineering cell shape and function. Science 1994; 264:696-8. [PMID: 8171320].

41. Mathur A, Ma Z, Loskill P, Jeeawoody S, Healy KE. In vitro cardiac tissue models: Current status and future prospects. Adv Drug Deliv Rev 2016; 96:203-13. [PMID: 26428618].

42. Bhatia SN, Yarmush ML, Toner M. Controlling cell interactions by micropatterning in co-cultures: hepatocytes and 3T3 fibroblasts. J Biomed Mater Res 1997; 34:189-99. [PMID: 9029299].

43. Liu W-W, Chen Z-L, Jiang X-Y. Methods for Cell Micropatterning on Two-Dimensional Surfaces and Their Applications in Biology. Chin J Anal Chem 2009; 37:943-9. .

44. Vargis E, Peterson CB, Morrell-Falvey JL, Retterer ST, Collier CP. The effect of retinal pigment epithelial cell patch size on growth factor expression. Biomaterials 2014; 35:3999-4004. [PMID: 24485792].

45. Folch A, Jo BH, Hurtado O, Beebe DJ, Toner M. Microfabricated elastomeric stencils for micropatterning cell cultures. J Biomed Mater Res 2000; 52:346-53. [PMID: 10951374].

46. Zinchenko YS, Coger RN. Engineering micropatterned surfaces for the coculture of hepatocytes and Kupffer cells. J Biomed Mater Res A 2005; 75A:242-8. [PMID: 16052491].

47. Geisen P, McColm JR, King BM, Hartnett ME. Characterization of barrier properties and inducible VEGF expression of several types of retinal pigment epithelium in medium-term culture. Curr Eye Res 2006; 31:739-48. [PMID: 16966147].

48. Kamao H, Mandai M, Okamoto S, Sakai N, Suga A, Sugita S, Kiryu J, Takahashi M. Characterization of Human Induced Pluripotent Stem Cell-Derived Retinal Pigment Epithelium

Cell Sheets Aiming for Clinical Application. Stem Cell Rep 2014; 2:205-18. [PMID: 24527394].

49. Dunn KC, Aotaki-Keen AE, Putkey FR, Hjelmeland LM. ARPE-19, a human retinal pigment epithelial cell line with differentiated properties. Exp Eye Res 1996; 62:155-69. [PMID: 8698076].

50. Ablonczy Z, Dahrouj M, Tang PH, Liu Y, Sambamurti K, Marmorstein AD, Crosson CE. Human Retinal Pigment Epithelium Cells as Functional Models for the RPE In Vivo. Invest Ophthalmol Vis Sci 2011; 52:8614-20. [PMID: 21960553].

51. Derycke LDM, Bracke ME. N-cadherin in the spotlight of cell-cell adhesion, differentiation, embryogenesis, invasion and signalling. Int J Dev Biol 2004; 48:463-76. [PMID: 15349821].

52. Lagunowich LA, Grunwald GB. Tissue and age-specificity of post-translational modifications of N-cadherin during chick embryo development. Differ Res Biol Divers. 1991; 47:19-27. [PMID: 1916067].

53. Wheelock MJ, Johnson KR. Cadherins as modulators of cellular phenotype. Annu Rev Cell Dev Biol 2003; 19:207-35. [PMID: 14570569].

54. Gumbiner BM. Cell Adhesion: The Molecular Basis of Tissue Architecture and Morphogenesis. Cell 1996; 84:345-57. [PMID: 8608588].

55. Lagunowich LA, Grunwald GB. Expression of calcium-dependent cell adhesion during ocular development: a biochemical, histochemical and functional analysis. Dev Biol 1989; 135:158-71. [PMID: 2475376].

56. Hülsken J, Birchmeier W, Behrens J. E-cadherin and APC compete for the interaction with beta-catenin and the cytoskeleton. J Cell Biol 1994; 127:2061-9. [PMID: 7806582].

57. Funayama N, Fagotto F, McCrea P, Gumbiner BM. Embryonic axis induction by the armadillo repeat domain of beta-catenin: evidence for intracellular signaling. J Cell Biol 1995; 128:959-68. [PMID: 7876319].

58. Aberle H, Schwartz H, Kemler R. Cadherin-catenin complex: protein interactions and their implications for cadherin function. J Cell Biochem 1996; 61:514-23. [PMID: 8806074].

59. Furuse M, Fujita K, Hiiragi T, Fujimoto K, Tsukita S. Claudin-1 and −2: novel integral membrane proteins localizing at tight junctions with no sequence similarity to occludin. J Cell Biol 1998; 141:1539-50. [PMID: 9647647].

60. Nishiyama K, Sakaguchi H, Hu JG, Bok D, Hollyfield JG. Claudin localization in cilia of the retinal pigment epithelium. Anat Rec 2002; 267:196-203. [PMID: 12115268].

61. Anderson JM. Cell signalling: MAGUK magic. Curr Biol 1996; 6:382-4. [PMID: 8723338].

62. Schmitt M, Horbach A, Kubitz R, Frilling A, Häussinger D. Disruption of hepatocellular tight junctions by vascular endothelial growth factor (VEGF): a novel mechanism for tumor invasion. J Hepatol 2004; 41:274-83. [PMID: 15288477].

63. Fischer S, Wobben M, Marti HH, Renz D, Schaper W. Hypoxia-Induced Hyperpermeability in Brain Microvessel Endothelial Cells Involves VEGF-Mediated Changes in the Expression of Zonula Occludens-1. Microvasc Res 2002; 63:70-80. [PMID: 11749074].

64. Morin-Brureau M, Lebrun A, Rousset M-C, Fagni L, Bockaert J, de Bock F, Lerner-Natoli M. Epileptiform Activity Induces Vascular Remodeling and Zonula Occludens 1 Downregulation in Organotypic Hippocampal Cultures: Role of VEGF Signaling Pathways. J Neurosci 2011; 31:10677-88. [PMID: 21775611].

65. Leung JCK, Chan LYY, Li FFK, Tang SCW, Chan KW, Chan TM, Lam MF, Wieslander A, Lai KN. Glucose degradation products downregulate ZO-1 expression in human peritoneal mesothelial cells: the role of VEGF. Nephrol Dial Transplant 2005; 20:1336-49. [PMID: 15814533].

66. Antonetti DA, Barber AJ, Hollinger LA, Wolpert EB, Gardner TW. Vascular endothelial growth factor induces rapid phosphorylation of tight junction proteins occludin and zonula occluden 1. A potential mechanism for vascular permeability in diabetic retinopathy and tumors. J Biol Chem 1999; 274:23463-7. [PMID: 10438525].

67. Chidiac R, Zhang Y, Tessier S, Faubert D, Delisle C, Gratton J-P. Comparative Phosphoproteomics Analysis of VEGF and Angiopoietin-1 Signaling Reveals ZO-1 as a Critical Regulator of Endothelial Cell Proliferation. Mol Cell Proteomics 2016; 15:1511-25. [PMID: 26846344].

68. Steger C. An unbiased detector of curvilinear structures. IEEE Trans Pattern Anal Mach Intell 1998; 20:113-25. .

69. Kannan R, Sreekumar PG, Hinton DR. VEGF and PEDF Secretion in ARPE-19 and fhRPE Cells. Invest Ophthalmol Vis Sci 2011; 52:9047-[PMID: 22104197].

70. Georgiadis A, Tschernutter M, Bainbridge JWB, Balaggan KS, Mowat F, West EL, Munro PMG, Thrasher AJ, Matter K, Balda MS, Ali RR. The Tight Junction Associated Signalling Proteins ZO-1 and ZONAB Regulate Retinal Pigment Epithelium Homeostasis in Mice. PLoS One 2010; 5:e15730-[PMID: 21209887].

71. González-Mariscal L, Tapia R, Chamorro D. Crosstalk of tight junction components with signaling pathways. Biochim Biophys Acta BBABiomembr 2008; 1778:729-56. [PMID: 17950242].

72. Ghassemifar R, Lai C-M, Rakoczy PE. VEGF differentially regulates transcription and translation of ZO-1α+. Cell Tissue Res 2005; 323:117-25. [PMID: 16163490].

73. Katsuno T, Umeda K, Matsui T, Hata M, Tamura A, Itoh M, Takeuchi K, Fujimori T, Nabeshima Y, Noda T, Tsukita S, Tsukita S. Deficiency of Zonula Occludens-1 Causes Embryonic Lethal Phenotype Associated with Defected Yolk Sac Angiogenesis and Apoptosis of Embryonic Cells. Mol Biol Cell 2008; 19:2465-75. [PMID: 18353970].

74. Faehling M, Kroll J, Föhr KJ, Fellbrich G, Mayr U, Trischler G, Waltenberger J. Essential role of calcium in vascular endothelial growth factor A-induced signaling: mechanism of the antiangiogenic effect of carboxyamidotriazole. FASEB

J Off Publ Fed Am Soc Exp Biol. 2002; 16:1805-7. [PMID: 12354692].

75. Sunness JS, Gonzalez-Baron J, Bressler NM, Hawkins B, Applegate CA. The development of choroidal neovascularization in eyes with the geographic atrophy form of age-related macular degeneration. Ophthalmology 1999; 106:910-9. [PMID: 10328389].

76. McLeod DS, Taomoto M, Otsuji T, Green WR, Sunness JS, Lutty GA. Quantifying changes in RPE and choroidal vasculature in eyes with age-related macular degeneration. Invest Ophthalmol Vis Sci 2002; 43:1986-93. [PMID: 12037009].

77. Saint-Geniez M, Kurihara T, Sekiyama E, Maldonado AE, D'Amore PA. An essential role for RPE-derived soluble VEGF in the maintenance of the choriocapillaris. Proc Natl Acad Sci USA 2009; 106:18751-6. [PMID: 19841260].

78. Ishida S, Usui T, Yamashiro K, Kaji Y, Amano S, Ogura Y, Hida T, Oguchi Y, Ambati J, Miller JW, Gragoudas ES, Ng Y-S, D'Amore PA, Shima DT, Adamis AP. VEGF164-mediated Inflammation Is Required for Pathological, but Not Physiological, Ischemia-induced Retinal Neovascularization. J Exp Med 2003; 198:483-9. [PMID: 12900522].

Articles are provided courtesy of Emory University and the Zhongshan Ophthalmic Center, Sun Yat-sen University, P.R. China. The print version of this article was created on 17 July 2017. This reflects all typographical corrections and errata to the article through that date. Details of any changes may be found in the online version of the article.